PNAS RESEARCH ARTICLE | PHYSIOLOGY OPEN ACCESS

Oxygen regulation of breathing is abolished in mitochondrial complex III-deficient arterial chemoreceptors

Daniel Cabello-Rivera[a,b,c,1], Patricia Ortega-Sáenz[a,b,c,1,2], Lin Gao[a,b,c], Ana M. Muñoz-Cabello[a,b,c], Victoria Bonilla-Henao[a,b,c], Paul T. Schumacker[d], and José López-Barneo[a,b,c,2]

Edited by Bruce Bean, Harvard Medical School, Boston, MA; received February 7, 2022; accepted August 11, 2022

Acute oxygen (O_2) sensing is essential for adaptation of organisms to hypoxic environments or medical conditions with restricted exchange of gases in the lung. The main acute O_2-sensing organ is the carotid body (CB), which contains neurosecretory chemoreceptor (glomus) cells innervated by sensory fibers whose activation by hypoxia elicits hyperventilation and increased cardiac output. Glomus cells have mitochondria with specialized metabolic and electron transport chain (ETC) properties. Reduced mitochondrial complex (MC) IV activity by hypoxia leads to production of signaling molecules (NADH and reactive O_2 species) in MCI and MCIII that modulate membrane ion channel activity. We studied mice with conditional genetic ablation of MCIII that disrupts the ETC in the CB and other catecholaminergic tissues. Glomus cells survived MCIII dysfunction but showed selective abolition of responsiveness to hypoxia (increased [Ca^{2+}] and transmitter release) with normal responses to other stimuli. Mitochondrial hypoxic NADH and reactive O_2 species signals were also suppressed. MCIII-deficient mice exhibited strong inhibition of the hypoxic ventilatory response and altered acclimatization to sustained hypoxia. These data indicate that a functional ETC, with coupling between MCI and MCIV, is required for acute O_2 sensing. O_2 regulation of breathing results from the integrated action of mitochondrial ETC complexes in arterial chemoreceptors.

acute O_2 sensing | hypoxia | carotid body glomus cell | mitochondrial O_2 sensing and signaling | mitochondrial complex III

Molecular oxygen (O_2) is required for ATP synthesis by oxidative phosphorylation and is therefore essential for the maintenance of most life forms, particularly mammals (1). A reduction of arterial O_2 tension (hypoxemia) triggers life-saving acute respiratory and cardiocirculatory reflexes that minimize the deleterious effect of O_2 deficiency (2). The prototypical acute O_2-sensing organ is the carotid body (CB), a highly perfused structure located in the carotid bifurcation that contains neuron-like chemoreceptor glomus cells innervated by sensory fibers of the petrosal ganglion. Glomus cells are presynaptic-like elements in which hypoxia induces depolarization, Ca^{2+} influx, and the release of transmitters that stimulate afferent fibers impinging on the brainstem respiratory and autonomic centers. CB activation elicits hyperventilation and increased cardiac output to favor O_2 uptake and its distribution to the tissues (3, 4).

Although the electrophysiology of glomus cells and their responses to hypoxia are well known (3–6), the basic physiological mechanisms underlying acute O_2 sensing have remained elusive. While various hypotheses proposed to date have appeared attractive (4, 7), none have received strong experimental support as the ablation of genes coding relevant enzymes or receptors have resulted in mice lacking major alterations in CB responsiveness to hypoxia (8–12). A potential role of the mitochondria in CB O_2 sensing was classically suggested in response to the potent sensitivity of glomus cells to mitochondrial inhibitors (13) and the modulation of some mitochondrial parameters by O_2 tension (14, 15). In addition, rotenone, a mitochondrial complex (MC) I inhibitor, was found to mimic and occlude any further effect of hypoxia (16). However, the manner by which mitochondria sense hypoxia and transduce this signal to affect membrane ion channels remained unresolved until recently, when glomus cell gene-expression analyses (17, 18), as well as the study of new genetically modified mouse models (19–21), led us to propose a "mitochondrial to membrane signaling" (MMS) model of CB acute O_2 sensing. This model, which integrates the membrane and mitochondrial responses to hypoxia, suggests that glomus cells exhibit a highly active mitochondrial metabolism and electron transport chain (ETC) combined with a relatively low apparent affinity of cytochrome *c* oxidase for O_2 arising from HIF2α-dependent expression of specific mitochondrial enzymes and atypical MCIV subunit isoforms (18, 21). In response to relatively mild levels of hypoxia, the decrease in cytochrome *c* oxidase activity would cause a backup of electrons along the ETC, thereby

Significance

Oxygen sensing by chemoreceptor glomus cells in the carotid body plays an essential adaptive function in health and disease; however, the underlying mechanisms are not fully understood. Glomus cells survive genetic disruption of mitochondrial complex III, although this results in a functional disconnection between the distal and proximal components of the mitochondrial electron transport chain (ETC). These cells exhibit selective abolition of mitochondrial and cellular responsiveness to hypoxia, as well as altered systemic hyperventilation and acclimatization to hypoxia, indicating that acute oxygen-sensing and -signaling during hypoxia result from the integrated action of mitochondrial ETC components. The mitochondrial ETC emerges as a complex oxygen-sensing and -signaling system of potential pathophysiological relevance in maladaptive responses to hypoxia.

Author contributions: D.C.-R., P.O.-S., L.G., A.M.M.-C., and J.L.-B. designed research; D.C.-R., P.O.-S., L.G., and V.B.-H. performed research; P.T.S. provided essential material for the research; D.C.-R., P.O.-S., L.G., A.M.M.-C., and V.B.-H. analyzed data; and D.C.-R., P.O.-S., L.G., A.M.M.-C., P.T.S., and J.L.-B. wrote the paper.

The authors declare no competing interest.

This article is a PNAS Direct Submission.

[1]D.C.-R. and P.O.-S. contributed equally to this work.

[2]To whom correspondence may be addressed. Email: gortega1@us.es or lbarneo@us.es.

This article contains supporting information online at http://www.pnas.org/lookup/suppl/doi:10.1073/pnas.2202178119/-/DCSupplemental.

Published September 19, 2022.

resulting in a highly reduced MCIII, an increased ratio of quinol (QH_2) to quinone (Q) and a slowdown (or even reversal) of MCI resulting in the accumulation of NADH and the production of reactive oxygen species (ROS). The increased mitochondrial NADH and ROS are transmitted to the cytosol to modulate the activity of ion channels responsible for cell depolarization (19–21).

A critical step toward a complete definition of the role of mitochondria in acute O_2 sensing and signaling is the analysis of the physiological responses to hypoxia of glomus cells in which MCI and MCIV are functionally disconnected. In these mitochondria, the redox status of the proximal mitochondrial ETC elements (MCI and quinone pool) is dissociated from changes in O_2-dependent MCIV activity, thus making it possible to test whether MCI signaling has intrinsic O_2 sensitivity or requires coupling to MCIV activity. To this end, we have studied a mouse model in which the gene encoding the Rieske iron-sulfur protein (RISP), a key component of MCIII necessary for the transfer of electrons from QH_2 to cytochrome *c* (22–25), is ablated in glomus cells and other catecholaminergic tissues (tyrosine hydroxylase [TH]-RISP mouse). Here, we show that TH-RISP mice exhibit a selective abolition of the hypoxic ventilatory response (HVR) and of mitochondrial and cellular responses to hypoxia in glomus cells. Responsiveness to other stimuli remained normal. These data strongly suggest that an integrated action of mitochondrial ETC complexes is required for acute O_2 sensing and signaling by arterial chemoreceptors.

Results

Generalized Catecholaminergic Neuronal Loss with Preservation of Peripheral Chemoreceptor Cells in TH-RISP Mice. We generated TH-RISP mice by breeding mice carrying lox-P–flanked exon 2 in the two *Uqcrfs1* gene alleles encoding the RISP subunit of MCIII ($RISP^{flox/flox}$) (25) with mice expressing Cre recombinase under the control of the TH promoter (TH-IRES-Cre mice) (26) (Fig. 1*A*). Newborn TH-RISP mice had a similar appearance to control ($RISP^{flox/+}$) littermates; however, 3 to 4 wk postnatally (P) they started to show a severe phenotype characterized by dwarfism, alterations in gait, and extreme lordosis (Fig. 1 *B* and *C*). These mice showed a decrease in serum levels of growth hormone (Fig. 1*D*). Because most of the TH-RISP mice died between days P45 and P50, experiments to evaluate systemic and cellular responsiveness to hypoxia were performed at ~P40, before the mice suddenly underwent deterioration of their general state. CBs dissected from TH-RISP mice had a marked and selective decrease in *Uqcrfs1* mRNA despite not all cells in the organ being TH^+, thus indicating a strong recombination induced by transgenic Cre (Fig. 1*E*). Histological analyses of the carotid bifurcations from TH-RISP mice showed CBs with a normal general structure and number of TH^+ glomus cells clustered in glomeruli (Fig. 1 *F* and *G*). In contrast, a clear atrophy of the neighboring superior cervical ganglion, with a marked decrease in the volume and density of TH^+ sympathetic neurons (Fig. 1 *F* and *H*) was observed. Similar to other mouse models with genetic disruption of genes encoding mitochondrial ETC subunits (27–30), we also observed a decrease in the number of TH^+ neurons in ventromedial hypothalamic areas of TH-RISP mice (possibly related to the observed mouse dwarfism) as well as in the dopaminergic nigrostriatal pathway (*SI Appendix*, Fig. S1). As the objective of this work was to study acute O_2 sensing by CB glomus cells, the potential neurodegenerative phenotype of the TH-RISP mice was not investigated further.

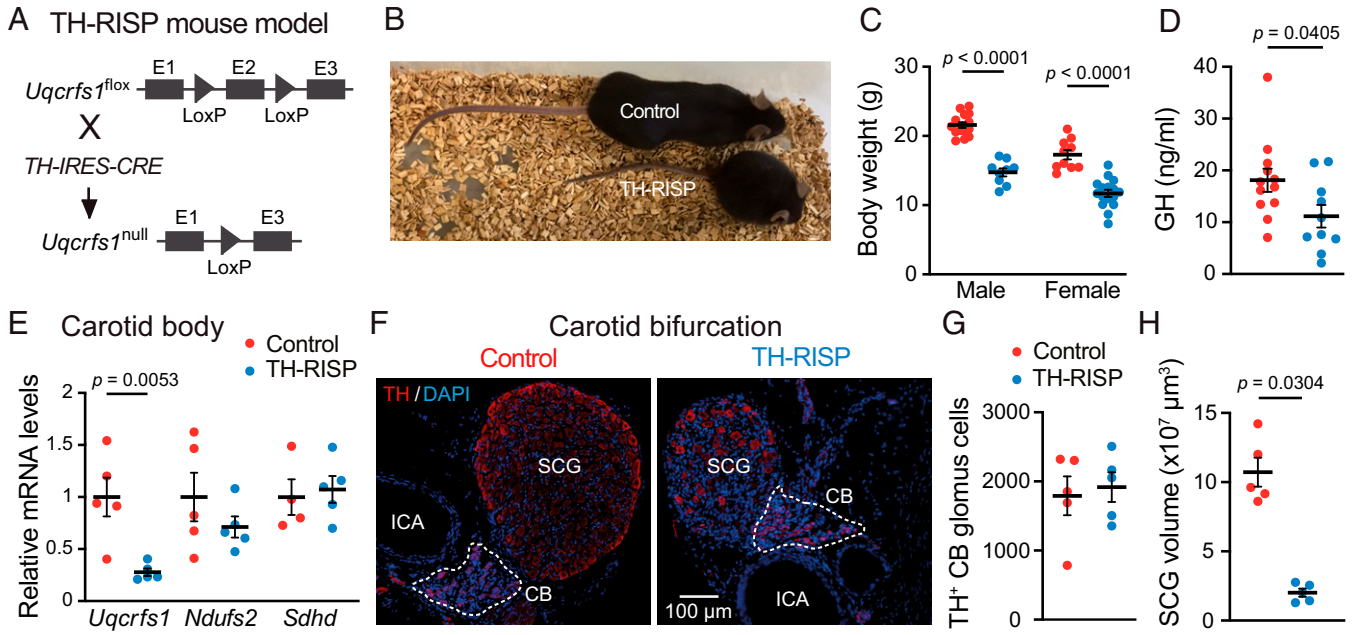

Fig. 1. General characteristics of TH-RISP mice. (*A*) Generation of the conditional TH-RISP mouse model. (*B*) Representative photograph of male control and TH-RISP mice (P40). (*C*) Body weight of control and TH-RISP mice at ~P40 (male: $n = 9$ to 15 mice per group; female: $n = 10$ to 16 mice per group). Data are expressed as mean ± SEM. Values are: 21.6 ± 0.4 g (male, control), 14.7 ± 0.6 g (male, TH-RISP), 17.3 ± 0.7 g (female, control), and 11.7 ± 0.5 g (female, TH-RISP). (*D*) Growth hormone (GH) levels in serum of control ($n = 12$) and TH-RISP ($n = 10$) mice (~P40). Data are expressed as mean ± SEM. Values are: 18.1 ± 2.2 ng/mL (control); 11.2 ± 2.2 ng/mL (TH-RISP). (*E*) *Uqcrfs1*, *Ndufs2*, and *Sdhd* mRNA levels expressed relative to control mice in CBs of control and TH-RISP mice ($n = 4$ to 5 mice per group). Data are expressed as mean ± SEM. From left to right values are: 1 ± 0.2; 0.3 ± 0.04; 1 ± 0.2; 0.7 ± 0.1; 1 ± 0.17; 1.1 ± 0.13). (*F*) Immunofluorescence detection of TH (red) in carotid artery bifurcations from control and TH-RISP mice. The white broken line delimits CB perimeter. ICA, internal carotid artery; SCG, superior cervical ganglion. Nuclei were counterstained with DAPI (blue). (*G*) Quantification of the number of CB TH^+ cells of control (1,792 ± 280, $n = 5$) and TH-RISP (1,918 ± 214, $n = 5$) mice. (*H*) Total SCG volume measured in control (10.7 ± 1 × 10^7 μm^3, $n = 5$) and TH-RISP (2.01 ± 0.3 × 10^7 μm^3, $n = 5$) mice. Data are expressed as mean ± SEM *P* values are indicated when data were significantly different ($P < 0.05$; unpaired Student's *t* test).

Selective Abolition of Responsiveness to Hypoxia in RISP-Deficient Glomus Cells. The preservation of CBs in TH-RISP mice allowed us to study the responsiveness of single glomus cells to hypoxia. Exocytotic catecholamine release from control glomus cells in CB slices was monitored using an amperometric carbon-fiber electrode (Fig. 2*A*) (16), with basal secretory levels and responses to high K^+ similar to those recorded in previous studies in our laboratory (Fig. 2 *B*, *D*, and *E*) (19, 20). In this set of experiments, all CB cells from control mice that were activated by direct depolarization with K^+ were also activated by hypoxia, as well by other glomus cell stimuli such as hypercapnia and hypoglycemia (19) (Fig. 2 *F* and *G*). In contrast, RISP-deficient glomus cells were practically insensitive to hypoxia, although they showed normal, or even slightly potentiated, responses to K^+, hypercapnia, and hypoglycemia (Fig. 2 *C*–*G*). Only 1 of the 10 RISP-deficient cells studied that were activated by high K^+, hypercapnia, and hypoglycemia showed a response to hypoxia, although with a secretion rate that was below 50% of the average secretion rate measured in control cells (Fig. 2 *F* and *G*). The selective abolition of acute responsiveness to hypoxia in RISP-deficient CBs was confirmed in parallel microfluorimetric experiments performed with Fura-2–loaded dispersed glomus cells to record the hypoxia-induced changes in cytosolic $[Ca^{2+}]$ (19, 31). In agreement with the amperometric data described above, RISP-deficient glomus cells showed normal cytosolic Ca^{2+} responses to high K^+ and hypercapnia but were unresponsive to hypoxia (*SI Appendix*, Fig. S2). These data demonstrate that CB chemoreceptor cells can survive and adapt to impaired MCIII activity, maintaining their excitability and basic secretory functions as well as their responses to physiological stimuli, such as hypercapnia or hypoglycemia. However, MCIII-deficient glomus cells are insensitive to acute changes in O_2 tension.

Inhibition of Mitochondrial ETC-Dependent Hypoxic Signaling in RISP-Deficient Glomus Cells. Given that reactions along the mitochondrial ETC are reversible (with the exception of the generation of H_2O in MCIV) (32), it has been suggested that decreases in glomus cell cytochrome *c* oxidase activity in hypoxia causes a backup of electrons along the ETC. This results in the accumulation of NADH and an increase in ROS production due to an increase in the QH_2/Q ratio and the slow down or reversal of MCI, as well as the leak of electrons from a highly reduced MCIII (Fig. 3*A*) (19–21). To confirm that the ETC was actually interrupted in RISP-deficient mitochondria (Fig. 3*B*), we tested the effect of cyanide, an inhibitor of cytochrome *c* oxidase and potent CB glomus cell activator (16). Cyanide produced a strong secretory response in glomus cells from control mice (Fig. 3*C*); however, cells from TH-RISP mice were insensitive to cyanide and hypoxia although they showed a robust response to hypercapnia and hypoglycemia (Fig. 3*D*). These results indicate that MCIV is functionally separated from proximal components (MCI and the quinone pool) of the ETC in RISP-deficient glomus cells.

To further determine the impact of ETC interruption on glomus cell acute O_2 sensing and signaling, we monitored

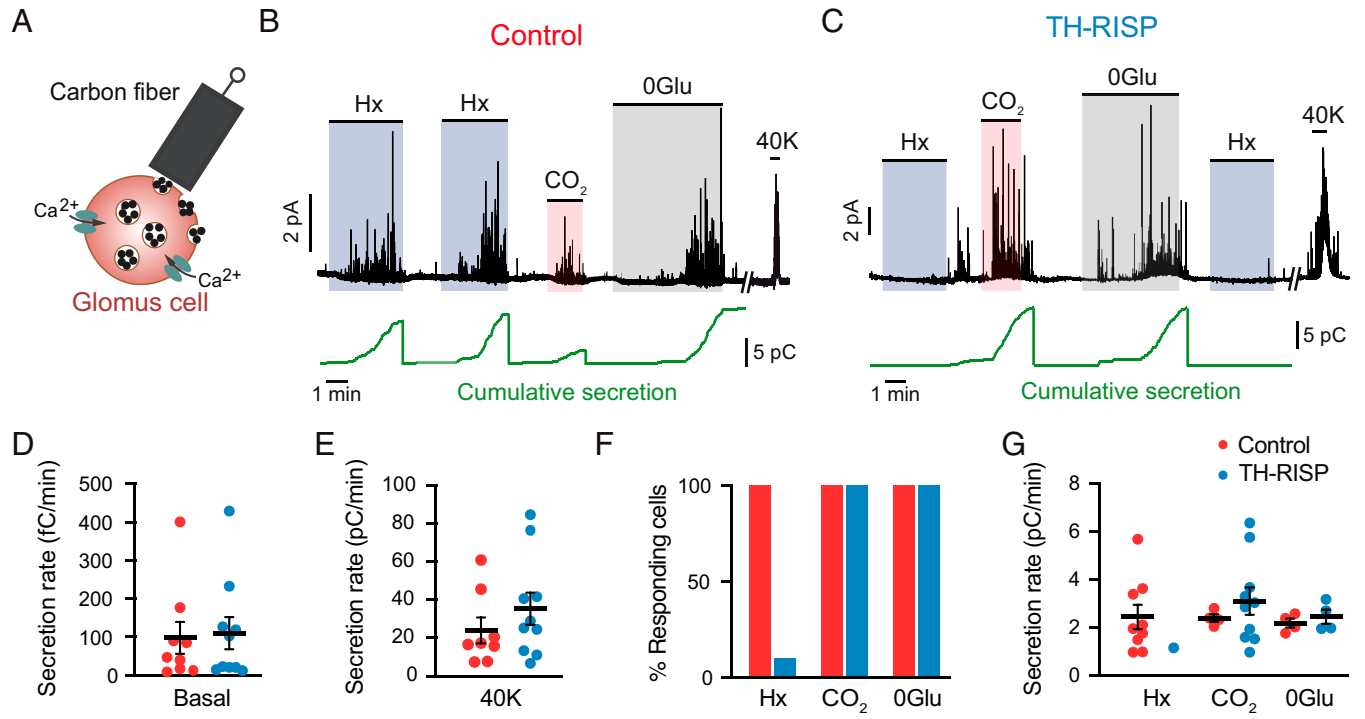

Fig. 2. Selective abolition of the secretory response to hypoxia in MCIII-deficient glomus cells. (*A*) Scheme illustrating the monitorization of quantal catecholamine release from single glomus cells by amperometry. (*B* and *C*) Representative amperometric recordings of secretory activity induced by hypoxia (Hx, O_2 tension ~15 mmHg), hypercapnia (20% CO_2), hypoglycemia (0 glucose, 0Glu), and depolarization with high potassium (40 mM K) in glomus cells from control (*B*) and TH-RISP (*C*) mice. Cumulative secretion signals are shown below each trace (green). The vertical lines indicate resetting of the integrator. (*D* and *E*) Quantification of the secretion rate of glomus cells in basal condition (*D*) and in response to 40 mM K (*E*). Data are expressed as mean ± SEM. Values of basal secretion are: control (red) cells, 97.7 ± 42 fC/min, n = 9 cells/7 mice; RISP-deficient (blue) cells, 110.3 ± 42.1 fC/min, n = 10 cells/7 mice. Values of high K-induced secretion are: control cells, 24 ± 7 pC/min, n = 9 cells/7 mice; RISP-deficient cells, 35.3 ± 8.4 pC/min, n = 10 cells/7 mice. P = 0.34; unpaired Student's t test. (*F*) Percentage of glomus cells with a secretory response to hypoxia (Hx), 0 mM glucose (0 Glu), and hypercapnia (CO_2) in control and TH-RISP mice. (*G*) Average secretion rate (pC/min) of glomus cells in response to hypoxia, hypercapnia and hypoglycemia. Data are expressed as mean ± SEM. Values are: hypoxia control (2.4 ± 0.5, n = 9 cells/7 mice); hypoxia TH-RISP (1.2, n = 1 cell); hypercapnia control (2.4 ± 0.2, n = 4 cells/4 mice); hypercapnia TH-RISP (3.1 ± 0.6, n = 10 cells/7 mice), P = 0.46; unpaired Student's t test; 0Glu control (2.2 ± 0.2, 4 cells/3 mice); 0Glu TH-RISP (2.5 ± 0.3, 4 cells/3 mice), P = 0.47; unpaired Student's t test.

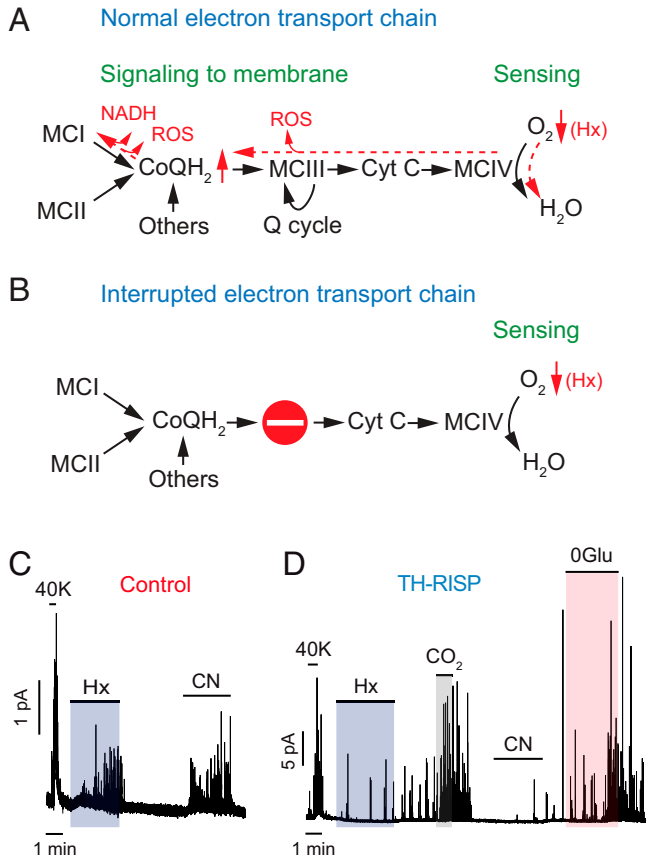

Fig. 3. Interruption of the mitochondrial electron transport chain and abolition of responsiveness to cyanide in MCIII-deficient glomus cells. (*A* and *B*) Scheme of the ETC and dynamic changes (in red) induced by hypoxia (Hx) (*A*). The stop signal indicates interruption of the ETC in RISP-deficient cells (*B*). $CoQH_2$, reduced ubiquinone); Cyt C, cytochrome *c*; Q cycle, quinone cycle. (*C*) Representative amperometric recordings of the secretory activity induced by high K (40K), hypoxia (Hx), and cyanide (200 μM) in glomus cells from control mice. Similar results were obtained in four cells/three mice tested. (*D*) Representative amperometric recordings of the secretory activity induced by the same stimuli tested in (*C*), plus 0Glu and hypercapnia (CO_2), in a RISP-deficient glomus cell. Note in *D* the selective inhibition of responsiveness to hypoxia and cyanide. Similar results were obtained in six cells/three mice tested.

changes in NADH and mitochondrial ROS in response to hypoxia, as these are signals that have been proposed to modulate membrane ion channel activity leading to cell depolarization and transmitter release (19, 20). Characteristic hypoxia-induced reversible increases in NADH (14, 19) were recorded in almost 90% of wild-type glomus cells studied (Fig. 4 *A* and *C–E*). In contrast, this response was practically abolished in RISP-deficient glomus cells (Fig. 4 *B* and *C–E*). In the relatively few responsive cells that were identified (less than 20%) (Fig. 4*D*), the effect of hypoxia was much smaller than in controls (Fig. 4*E*). In all wild-type (n = 14/4 mice) and hypoxia-unresponsive RISP-null (n = 16/3 mice) cells tested, the application of α-ketobutyrate (αKB), which is transported and converted to nonmetabolizable α-hydroxybutyrate by NADH-consuming dehydrogenases expressed in normal glomus cells (20, 33, 34), produced a clear decrease in NADH autofluorescence (Fig. 4 *A*, *B*, and *F*). The decrease in intracellular NADH induced by αKB resulted in selective and reversible abolition of the secretory response induced by hypoxia (Fig. 4*G*). Notably, basal levels of NADH in RISP-deficient glomus cells were slightly decreased with respect to controls (Fig. 4*C*), suggesting that these cells, although possessing a dysfunctional ETC, have a conserved mitochondrial pool (*SI Appendix*, Fig. S3), with repurposed metabolism to regenerate NAD^+. In agreement with this idea, rotenone (a selective blocker of MCI NADH dehydrogenase activity) produced an increase in NADH autofluorescence in both control and TH-RISP glomus cells (*Discussion* and Fig. 4 *H–K*).

Hypoxia-induced mitochondrial ROS signals were monitored with a redox-sensitive fluorescent protein probe (roGFP) that was genetically targeted to the intermembrane space (IMS) or the matrix (35). We have previously shown in CB slices infected with adenoviral vectors containing roGFP that hypoxia generates compartmentalized fast and reversible redox signals in glomus cells (20) (*SI Appendix*). Hypoxia-induced increases in IMS ROS were abolished in RISP-deficient glomus cells (Fig. 4 *L–P*), whereas hypoxia-induced decreases in matrix ROS remained unaltered (*SI Appendix*, Fig. S4). These data strongly support the concept that the reversible rise in IMS ROS is a response associated with acute hypoxic signaling by glomus cells and depends on the leak of electrons from reduced MCI and MCIII (20, 21). The fact that the hypoxia-induced reversible decrease in matrix ROS was maintained in RISP-deficient glomus cell mitochondria indicates that, as previously suggested (20), this signal is unrelated to acute hypoxia signaling; it may simply reflect a nonspecific phenomenon secondary to the decrease in O_2 available for superoxide production by matrix dehydrogenases (36, 37).

Abolition of the Ventilatory Response and Altered Acclimatization to Hypoxia in TH-RISP Mice. As is the case in humans (38), the HVR is practically abolished in mice without functional CBs (19, 39). In agreement with the data from single chemoreceptor cells, whole-body plethysmography experiments showed a complete disappearance of the HVR in TH-RISP mice, while the response to hypercapnia remained unchanged (Fig. 5 *A–D*). In TH-RISP mice, hypoxia even produced a significant decrease in breathing frequency (Fig. 5 *A* and *C*), a phenomenon that, in the absence of CB activation, may represent the inhibition of brainstem neurons by the reduction in blood O_2 tension (40). Basal breathing frequency under normoxic conditions was also consistently reduced (~15%) in TH-RISP mice compared to wild-type mice (Fig. 5*C*), which is probably a consequence of a decrease in the respiratory drive impinging on brain centers in mice with O_2-insenstive CBs. The lack of responsiveness to hypoxia observed in TH-RISP mice resulted in an alteration of systemic acclimatization to hypoxia. This was manifested by an exaggerated increase in hematocrit in TH-RISP animals maintained under conditions of sustained hypoxia (10% O_2 tension) for 10 to 14 d (Fig. 6*A*). An increased extramedullary erythropoiesis in RISP-deficient mice was probably the reason why they had a marked splenic enlargement in comparison with controls (Fig. 6 *B* and *C*).

Discussion

We have shown in the present study that genetic ablation of the gene coding for RISP, an essential subunit of MCIII (22–25), in CB catecholaminergic chemoreceptor cells abolishes acute O_2 sensing and acclimatization to hypoxia. Remarkably, CB glomus cells survived and maintained their characteristic TH^+ phenotype in the absence of a functional MCIII, while other peripheral and central catecholaminergic neurons were severely affected. Indeed, TH-RISP mice died within the first 7 to 8 wk of postnatal life. The analysis of biochemical adaptations occurring in MCIII-deficient glomus cells is beyond the objective of the present work;

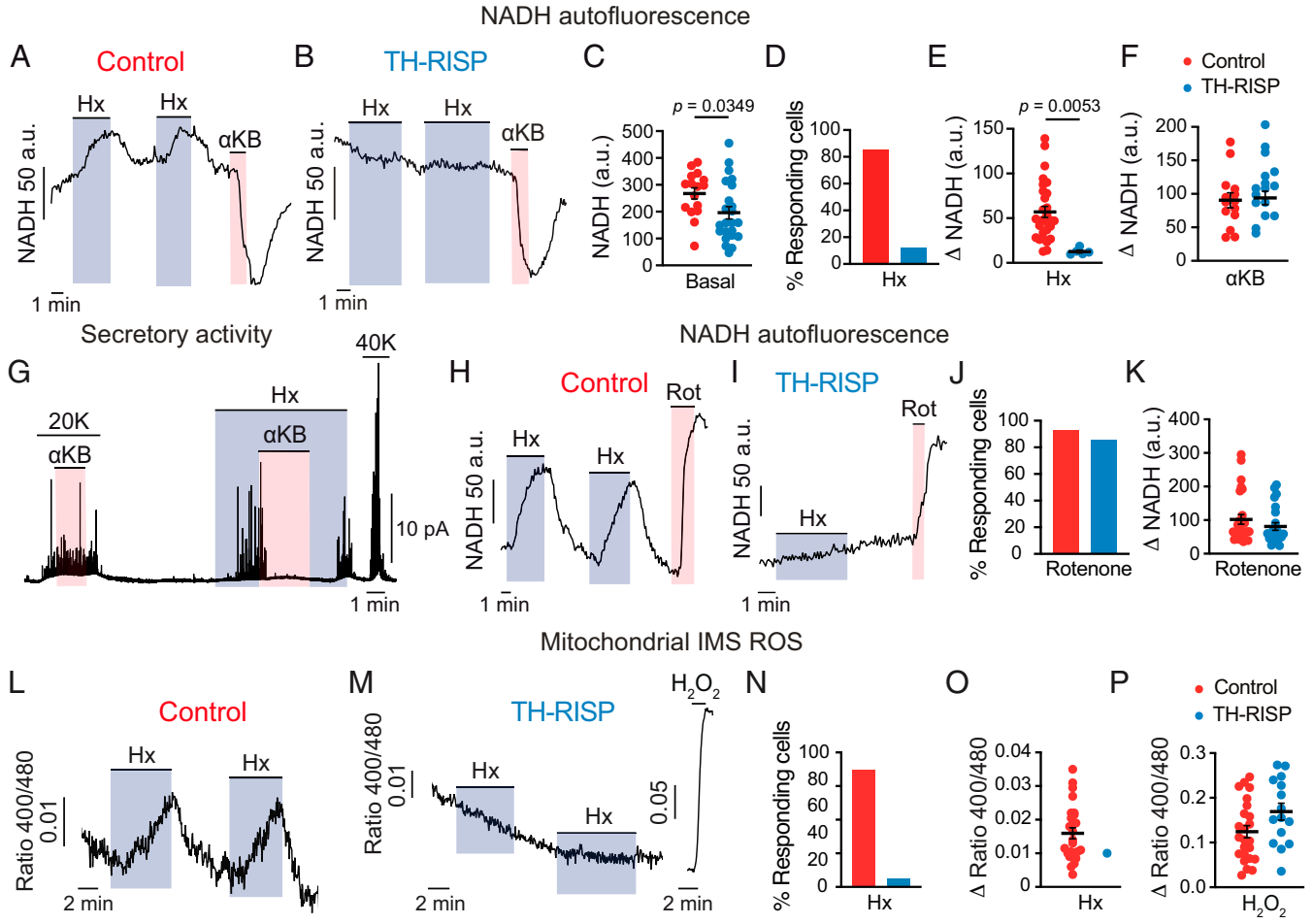

Fig. 4. Inhibition of hypoxia-induced mitochondrial signaling in MCIII-deficient glomus cells. (*A* and *B*) Representative recordings of changes in NADH in response to hypoxia and αKB in glomus cells from control (*A*) and TH-RISP (*B*) mice. (*C*) Basal NADH levels measured in control (268 ± 21 a.u., n = 33 cells/7 mice) and RISP-deficient (196 ± 23 a.u., n = 42 cells/7 mice) glomus cells. (*D*) Percentage of cells with a hypoxia-induced increase in NADH in control and TH-RISP mice. (*E*) Increase in NADH (Δ NADH) elicited by hypoxia (Hx, O_2 tension ~15 mm Hg) in control (57 ± 6 a.u., n = 29 cells/7 mice) and RISP-deficient (13 ± 2 a.u., n = 5 cells/7 mice) glomus cells. (*F*) Changes in NADH in response to αKB, 1 mM) in control (90 ± 11 a.u., n = 14 cells/4 mice) and RISP-deficient (93 ± 10 a.u., n = 16 cells/3 mice) glomus cells. (*G*) Representative recording illustrating the inhibition of the secretory response to hypoxia by αKB (1 mM) and the lack of effect of this agent on the secretory response to high K in a control glomus cell. Similar results obtained in n = 6 cells/4 mice for 20 mM K and n = 8 cells/5 mice for hypoxia (Hx, O_2 tension ~15 mmHg). (*H* and *I*) Representative recordings of NADH changes induced by hypoxia (Hx) and rotenone (Rot, 1 μM) in glomus cells from control (*H*) and TH-RISP (*I*) mice. (*J*) Percentage of cells with an increase in NADH induced by rotenone in control (red bar) and TH-RISP (blue bar) glomus cells. (*K*) Changes in NADH in response to rotenone (1 μM) in control (red symbols, 102 ± 14 a.u., n = 27 cells/5 mice) and RISP-deficient (blue symbols, 81 ± 11 a.u., n = 24 cells/5 mice) glomus cells. (*L* and *M*) Real-time changes ROS in the mitochondrial IMS induced by hypoxia (Hx) in control (*L*) and RISP-deficient (*M*) glomus cells. The response to 0.2 mM H_2O_2 was tested (in *M*) to ensure correct functioning of the mitochondrial roGFP probes. (*N*) Percentage of glomus cells with hypoxia induced increase in IMS ROS. Control mice (n = 30 cells/21 mice); TH-RISP mice (n = 17 cells/13 mice). (*O*) Hypoxia-induced increase in IMS ROS signal (Δ 400/480 ratio) in hypoxia-responsive glomus cells. Control cells (0.016 ± 0.002, n = 21 cells/17 mice); RISP-deficient cells (0.01, n = 1 cell/1 mouse). (*P*) Increase in IMS ROS (Δ 400/480 ratio) in response to 0.2 mM H_2O_2 in glomus cells. Control cells (0.124 ± 0.014, n = 24 cells/17 mice); RISP-deficient cells (0.169 ± 0.019, n = 15 cell/11 mice). In all panels data are expressed as mean ± SEM P values are indicated when data were significantly different ($P < 0.05$; unpaired Student's t test).

however, it is relevant to stress that RISP deficiency completely abolishes the transfer of electrons from QH_2 to cytochrome c (22–24). In agreement with these data, we showed that inhibition of MCIV with cyanide, a powerful glomus cell stimulant (16), does not activate RISP-null glomus cells, thus demonstrating interruption of the chemical connection between MCI and MCIV in their mitochondria. Therefore, it is possible that survival of RISP-deficient glomus cells, with MCI and MCII disconnected from MCIV, depends not only on the up-regulation of glycolytic ATP synthesis (19, 30) but also on remodeling of the mitochondrial ETC to utilize an electron acceptor alternative to O_2. In this regard, reversal of succinate dehydrogenase activity and utilization of fumarate as an electron acceptor are metabolic adaptations (41–43) that could support MCI activity in RISP-null glomus cells (see next paragraphs).

In TH-RISP mice with MCIII-deficient CB cells, acute effects of hypoxia on mitochondrial (NADH and ROS signals), cellular (increased cytosolic Ca^{2+} and catecholamine release), and systemic (increased breathing frequency) processes were abolished selectively. However, the cellular and systemic actions of other stimuli (high K^+, hypercapnia, or hypoglycemia) remained unaltered. These findings indicate that a functional mitochondrial ETC is absolutely required for glomus cell responsiveness to hypoxia and strongly support the view that, as suggested by the MMS model (19, 21), the integrated action of the various mitochondrial complexes is necessary for acute O_2 sensing and signaling. Indeed, genetic ablation of essential MCI (19) and MCII (18) subunits also abolishes responsiveness of glomus cells to hypoxia. Moreover, classic pharmacological studies in anesthetized cats showed that inhibition of ETC with

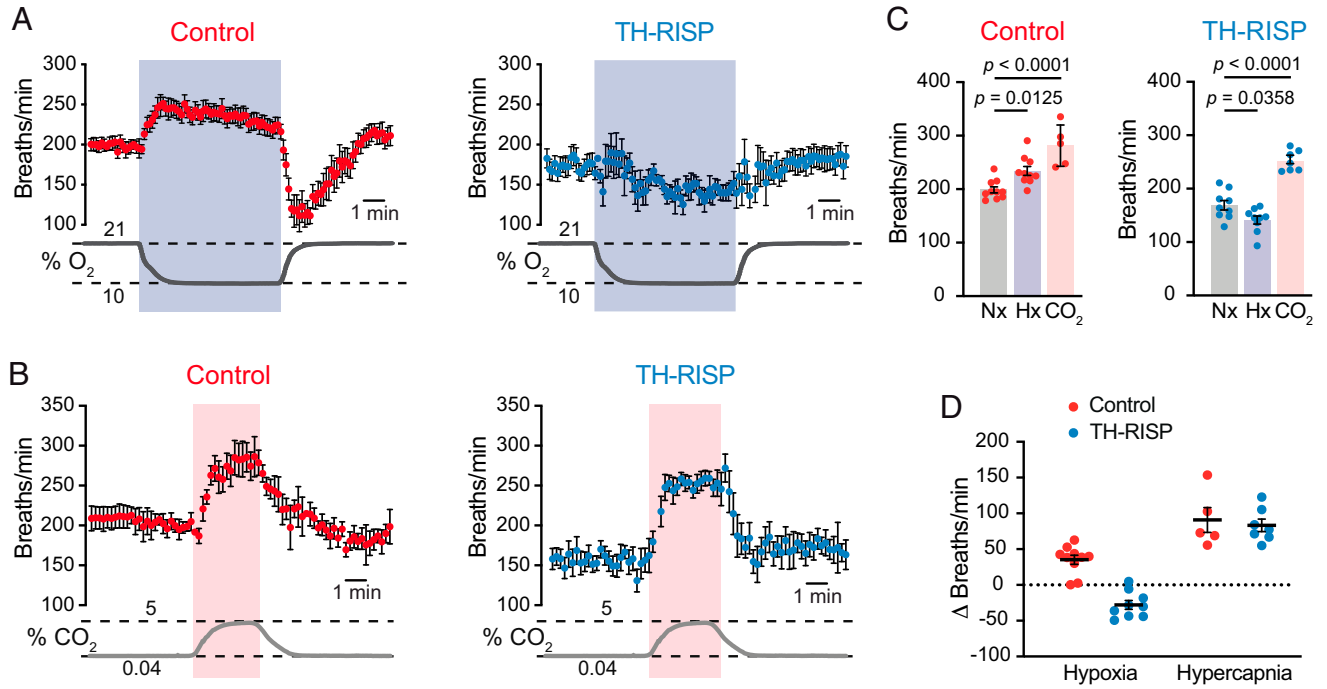

Fig. 5. Inhibition of the hypoxic ventilatory response in TH-RISP mice. (*A* and *B*) Average time course of plethysmographic recordings illustrating the increase in respiratory frequency induced by hypoxia (10% O_2) (*A*) and hypercapnia (5% CO_2) (*B*) in control and TH-RISP mice. Changes in air O_2 and CO_2 levels (in percent) are represented at the bottom of each panel. (*C*) Respiratory frequencies measured during normoxia (Nx), hypoxia (Hx), and hypercapnia (CO_2) in control and TH-RISP mice. Values (in breaths per minute) are: control (normoxia, 199 ± 6, n = 10; hypoxia, 234 ± 8, n = 10; CO_2, 281 ± 17, n = 5); TH-RISP (normoxia, 169 ± 9, n = 9; hypoxia, 141 ± 8, n = 9; CO_2, 252 ± 7, n = 7). (*D*) Average increase in respiratory frequency relative to basal values measured during exposure to hypoxia and hypercapnia in control and TH-RISP mice. Values (in Δ breaths per minute) are: hypoxia (control, 35 ± 6, n = 10; TH-RISP, −28 ± 6, n = 9); hypercapnia (control, 91 ± 17, n = 5; TH-RISP, 83 ± 9, n = 7). Data are expressed as mean ± SEM *P* values are indicated in the figure when data were significantly different ($P < 0.05$; paired one-way ANOVA).

oligomycin (a mitochondrial poison that blocks ATP synthesis) suppresses CB responsiveness to hypoxia without altering sensitivity to hypercapnia (44). However, large doses of oligomycin attenuated carotid body chemoreceptor response to CO_2 as well (44), suggesting that the effect on O_2 sensing was not specific to the ATP production.

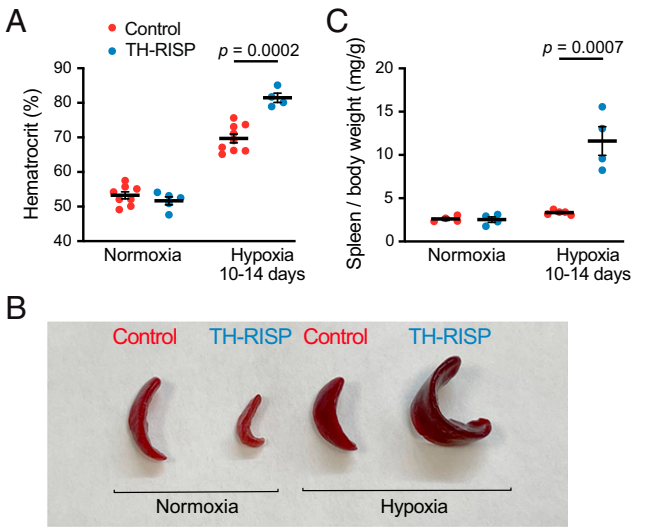

Fig. 6. Altered acclimatization to hypoxia in TH-RISP mice. (*A*) Increase in hematocrit during chronic hypoxia (10 to 14 d in 10% O_2) in control and TH-RISP mice (P25). Values are: normoxia (control, 53 ± 1%, n = 8; TH-RISP, 52 ± 1%, n = 5); hypoxia (control, 70 ± 1%, n = 9; TH-RISP, 81 ± 1%, n = 4). (*B*) Representative photographs of spleen from control and TH-RISP mice maintained in normoxia or in chronic hypoxia. (*C*) Quantification of spleen weight relative to body weight in normoxic and chronic hypoxic mice. Values are: normoxia (control, 2.6 ± 0.2 mg/g, n = 4; TH-RISP, 2.6 ± 0.3 mg/g, n = 4); hypoxia (control, 3.3 ± 0.1 mg/g, n = 5; TH-RISP, 11.6 ± 1.7 mg/g, n = 4). Data are expressed as mean± SEM *P* values are indicated when data were significantly different ($P < 0.05$; unpaired Student's *t* test).

Our data further demonstrate that O_2 and glucose, both of which are metabolic compounds essential for glomus cell homeostasis, are sensed by separate mechanisms (45). It is of note that compartmentalized mitochondrial ROS signals recorded during hypoxia (increase in the IMS and decrease in the matrix) (20) were differentially affected by the MCIII deficiency. While the IMS signal was abolished, the reversible decrease in matrix ROS was maintained in MCIII-null glomus cells. These results strongly suggest that the increase in IMS ROS, generated in MCI and MCIII, is associated with hypoxia signaling (20). Maintenance of the hypoxic matrix ROS signal in RISP-deficient cells indicates that their mitochondria are metabolically active even in the absence of MCIII. In support of this idea, we recorded decreased levels of NADH in MCIII-deficient cells in comparison with controls, while a marked increase in basal NADH is typically seen in MCI-deficient glomus cells (19). Moreover, rotenone (an MCI blocker) produced an increase in NADH levels both in control and TH-RISP cells. These findings suggest that MCIII-deficient glomus cell mitochondria have a functional MCI, which provides NAD^+ regenerative power, supplies QH_2 to reversed succinate dehydrogenase, and contributes to the inner membrane electrochemical proton gradient.

Within the context of the present discussion, it is relevant to indicate that hypoxia-induced compartmentalized ROS changes, qualitatively similar to those observed in CB glomus cells, have been described in O_2-sensitive cultured pulmonary arterial smooth muscle cells (PASMCs) (35), which mediate hypoxic pulmonary vasoconstriction (2). In those cultured cells,

ablation of the gene encoding RISP also selectively abolished the production of ROS at the IMS and the increase in cytosolic Ca^{2+} induced by hypoxia (25). Similar to CB glomus cells, PASMCs contain O_2-regulated ion channels, which seem to participate in the activation of these cells by hypoxia (2). Moreover, atypical MCIV subunit isoforms that modulate sensitivity to acute hypoxia are expressed in PASMCs (46, 47). Therefore, the MMS model of acute O_2 sensing proposed for CB glomus cells shares many features with mitochondria-mediated acute O_2 sensing in PASMCs, a process that has received much attention in recent times (2, 46, 48). However, whether hypoxia increases or decreases mitochondrial ROS production in PASMCs, and what might be the origin of the hypoxia-induced rise in cytosolic Ca^{2+}, have been matters of debate (35, 47, 49). It is also possible that some of the mechanisms underlying acute O_2 sensing in PASMCs differ from those operating in CB glomus cells. In this regard, it was shown that NDUFS2, a core subunit that is essential for MCI assembly and responsiveness of CB glomus cells to hypoxia (19, 20), is also necessary for the hypoxic activation of PASMCs (50). However, this last cited study reported that cysteine residues in NDUFS2 become reduced during acute hypoxia, thereby suggesting that structural changes in MCI may play a role in O_2 sensing. This conclusion contrasts with our current data, which indicate that although MCI seems to be active in MCIII-deficient cells, the signaling of hypoxia (accumulation of NADH and IMS ROS) requires a functional connection between MCI and MCIV. These observations argue against any intrinsic O_2 sensitivity of MCI.

In summary, we have shown that MCIII-deficient cells lose sensitivity to hypoxia while maintaining normal morphological and immunocytochemical features and responsiveness to other stimuli, such as high K^+, hypercapnia, and hypoglycemia. Mice with MCIII-deficient CB cells also exhibit a complete abolition of the HVR. Our findings indicate that the functional connection between MCI and MCIV is necessary for acute O_2 sensing by glomus cells. The CB-mediated O_2 regulation of breathing depends on an integrated action of the various components of the mitochondrial ETC and their ability to sense and signal hypoxia. Given the importance of CB in the regulation of breathing, mitochondrial ETC emerges as a potential therapeutic target for the pharmacological treatment of respiratory depression or CB overactivation (3, 51).

Materials and Methods

Mouse Models, Maintenance, and Treatments. Conditional MCIII knockout mice (TH-RISP) were generated breeding mice carrying *Uqcrfs1* floxed allele (25) with mice expressing Cre recombinase under the control of the TH promoter (26). TH-RISP mice and their control littermates were maintained in C57BL/6 genetic background. Mice were housed at a regulated temperature (22 ± 1 °C) in a 12-h light/12-h dark cycle with ad libitum access to food and water. Unless specified otherwise, both male and female mice of ∼40-d old were used in the present study. For chronic hypoxic treatment, 25-d-old mice were exposed to 10% O_2 for 10 to 14 d in a conventional hypoxic hermetic isobaric chamber with continuous monitoring of O_2, CO_2, humidity, and temperature (Coy Laboratory Products). Mice were killed with intraperitoneal administration of a lethal dose of sodium thiopental (120 to 150 mg/kg) before tissue dissection for in vitro functional, biochemical, or immunohistochemical analyses. Mice were maintained according to the European Community Council directives 86/609/EEC, and 2010/63/EU for the Care and Use of Laboratory Animals. All procedures were approved by the Ethics Committee of Animal Care and Use of Hospital Virgen del Rocío/Institute of Biomedicine of Seville (22-09-15-332; 07-04-2020-051). Additional information on mice genotyping and other procedures are given in *SI Appendix, Materials and Methods*.

Plethysmography. To study respiratory function, conscious unrestricted mice were placed in a plethysmography chamber as previously described (52). Chambers were perfused at 1 L/min of constant flow rate with normoxia (21% O_2), hypoxia (10% O_2, maintained for 5 min once O_2 percentage reached 10 oxygen), or hypercapnia (5% CO_2, maintained during 1 min when CO_2 percentage reached 5%). Data acquisition was performed using the Iox2 software from EMKA Technologies. O_2 and CO_2 sensors located inside the hermetic chambers allowed to monitor changes in gas composition in parallel with alterations in respiratory frequency recorded by a pressure sensor during the experiment.

Measurement of Hematocrit and Growth Hormone. After killing, blood was collected in some mice from an incision in the heart using a catheter. Details of hematocrit and growth hormone measurements are given in *SI Appendix, Materials and Methods*.

Preparation of CB Slices and Dispersed Glomus Cells. Mice were killed and carotid bifurcations were removed and placed in cold PBS where CB were dissected. Mouse CB slices and dispersed CB glomus cells were prepared as described previously by our laboratory (53–55). Slices were maintained at 37 °C in a 5% CO_2 incubator for 24 to 48 h prior to use. Freshly dispersed cells were plated on glass coverslips treated with poly-L-lysine (Sigma) and maintained at 37 °C in a 5% CO_2 incubator for 24 h before use. Additional information on the preparation and culture of CB dispersed cells and slices is given in *SI Appendix, Materials and Methods*.

Quantitative PCR. Carotid bifurcations were removed from mice after killing and placed in cold PBS where CBs were dissected. For RNA measurement, CBs were flash-frozen in liquid N_2 and stored at −80 °C until use. Total RNA was isolated from the CB with RNeasy Micro Kit (Qiagen) following the manufacturer's instruction. Complementary RNA (cRNA) was then amplified from total RNA using GeneChip WT Pico kit (Affymetrix). In total, 500 ng of cRNA was copied to cDNA using QuantiTect Reverse Transcription Kit (Qiagen). Real-time quantitative PCR reactions were performed in a 7500 Fast Real Time PCR System (Applied Biosystem) using Taqman Gene Expression Assays (Thermo Fisher Scientific) for each specific gene. Peptidylprolyl isomerase A (*Ppia*) was also estimated in each sample to normalize the amount of cRNA input in order to perform relative quantification.

Immunohistochemistry. Standard immunohistochemical analyses were done on sections of the carotid bifurcation and the brain following the procedures described in *SI Appendix, Materials and Methods*.

Amperometry. To record the secretory activity (catecholamine release) of glomus cells in CB slices we used the amperometry technique, as described previously in our laboratory (52, 53). Further details of this technique are given in *SI Appendix, Materials and Methods*.

Microfluorimetry. Microfluorimetric measurements in single dispersed glomus cells (Ca^{2+} and NADH) or cells in CB slices (mitochondrial ROS production) was performed following methods previously described (19, 20, 55). Specific details of these methodologies as used in this work are given in *SI Appendix, Materials and Methods*.

Recording Solutions. For amperometric and microfluorimetric experiments, CB slices or dispersed glomus cells were continuously perfused with a control solution containing 125 mM NaCl, 4.5 mM KCl, 23 mM $NaHCO_3$, 1 mM $MgCl_2$, 2.5 mM $CaCl_2$, 5 mM glucose, and 5 mM sucrose at ∼35 °C. In 40 mM K^+ solution, NaCl was replaced equimolarly with KCl. When 0 glucose solution was used, glucose was replaced equimolarly with sucrose. The "normoxic" solution was bubbled with a gas mixture of 20% O_2, 5% CO_2, and 75% N_2 (O_2 tension ∼145 mmHg). The "hypoxic" solution was bubbled with 5% CO_2 and 95% N_2 (O_2 tension in the recording chamber of ∼10 to 15 mmHg). Osmolality of solutions was ∼300 mosmol/kg.

Statistical Analysis. Data are presented as mean ± SEM. A Shapiro–Wilk test was used in order to verify that the dataset to be analyzed came from a normally distributed population. An unpaired Student's *t* test analysis was used for comparison between two datasets. Paired one-way ANOVA followed by the Tukey's

post hoc test were used when indicated. $P < 0.05$ was considered significant. Statistical analyses were performed using Prism 6.0 (GraphPad Software).

Data, Materials, and Software Availability. Data generated or analyzed over the course of this study are included within the main text or *SI Appendix*.

ACKNOWLEDGMENTS. This research was supported by the Andalusian Government (Fondos Feder US-1255654), Spanish Ministries of Science and Innovation and Health (Grants SAF2016-74990-R and PID2019-106410RB-I00 funded by MCIN/AEI/10.13039/501100011033), and the European Research Council (ERC Advanced Grant PRJ201502629). D.C.-R. received a predoctoral fellowship (FPU program) from the Spanish Government. We thank the staff of Institute of Biomedicine of Seville and "Centro de Producción y Experimentación Animal Oscar Pintado" for technical assistance.

Author affiliations: [a]Institute of Biomedicine of Seville (IBiS), Hospital Universitario Virgen del Rocío, Consejo Superior de Investigaciones Científicas, Universidad de Sevilla, Seville, 41013 Spain; [b]Department of Medical Physiology and Biophysics, University of Seville Medical School, 41009 Seville, Spain; [c]Centro de Investigación Biomédica en Red sobre Enfermedades Neurodegenerativas, 28031 Madrid, Spain; and [d]Department of Pediatrics, Northwestern University, Chicago, IL 60611

1. J. López-Barneo, M. C. Simon, Cellular adaptation to oxygen deficiency beyond the Nobel award. *Nat. Commun.* **11**, 607 (2020).
2. E. K. Weir, J. López-Barneo, K. J. Buckler, S. L. Archer, Acute oxygen-sensing mechanisms. *N. Engl. J. Med.* **353**, 2042–2055 (2005).
3. P. Ortega-Sáenz, J. López-Barneo, Physiology of the carotid body: From molecules to disease. *Annu. Rev. Physiol.* **82**, 127–149 (2020).
4. R. Iturriaga, J. Alcayaga, M. W. Chapleau, V. K. Somers, Carotid body chemoreceptors: Physiology, pathology, and implications for health and disease. *Physiol. Rev.* **101**, 1177–1235 (2021).
5. C. A. Nurse, Synaptic and paracrine mechanisms at carotid body arterial chemoreceptors. *J. Physiol.* **592**, 3419–3426 (2014).
6. N. R. Prabhakar, Y. J. Peng, G. K. Kumar, J. Nanduri, Peripheral chemoreception and arterial pressure responses to intermittent hypoxia. *Compr. Physiol.* **5**, 561–577 (2015).
7. R. J. Rakoczy, C. N. Wyatt, Acute oxygen sensing by the carotid body: A rattlebag of molecular mechanisms. *J. Physiol.* **596**, 2969–2976 (2018).
8. L. He *et al.*, Characteristics of carotid body chemosensitivity in NADPH oxidase-deficient mice. *Am. J. Physiol. Cell Physiol.* **282**, C27–C33 (2002).
9. P. Ortega-Sáenz, A. Pascual, R. Gómez-Díaz, J. López-Barneo, Acute oxygen sensing in heme oxygenase-2 null mice. *J. Gen. Physiol.* **128**, 405–411 (2006).
10. A. D. Mahmoud *et al.*, AMP-activated protein kinase deficiency blocks the hypoxic ventilatory response and thus precipitates hypoventilation and apnea. *Am. J. Respir. Crit. Care Med.* **193**, 1032–1043 (2016).
11. J. Wang, J. O. Hogan, R. Wang, C. White, D. Kim, Role of cystathionine-γ-lyase in hypoxia-induced changes in TASK activity, intracellular [Ca^{2+}] and ventilation in mice. *Respir. Physiol. Neurobiol.* **246**, 98–106 (2017).
12. H. Torres-Torrelo *et al.*, The role of Olfr78 in the breathing circuit of mice. *Nature* **561**, E33–E40 (2018).
13. E. Mulligan, S. Lahiri, Dependence of carotid chemoreceptor stimulation by metabolic agents on PaO_2 and $PaCO_2$. *J. Appl. Physiol.* **50**, 884–891 (1981).
14. M. R. Duchen, T. J. Biscoe, Mitochondrial function in type I cells isolated from rabbit arterial chemoreceptors. *J. Physiol.* **450**, 13–31 (1992).
15. K. J. Buckler, P. J. Turner, Oxygen sensitivity of mitochondrial function in rat arterial chemoreceptor cells. *J. Physiol.* **591**, 3549–3563 (2013).
16. P. Ortega-Sáenz, R. Pardal, M. García-Fernandez, J. López-Barneo, Rotenone selectively occludes sensitivity to hypoxia in rat carotid body glomus cells. *J. Physiol.* **548**, 789–800 (2003).
17. T. Zhou, M. S. Chien, S. Kaleem, H. Matsunami, Single cell transcriptome analysis of mouse carotid body glomus cells. *J. Physiol.* **594**, 4225–4251 (2016).
18. L. Gao *et al.*, Gene expression analyses reveal metabolic specifications in acute O_2-sensing chemoreceptor cells. *J. Physiol.* **595**, 6091–6120 (2017).
19. M. C. Fernández-Agüera *et al.*, Oxygen sensing by arterial chemoreceptors depends on mitochondrial complex I signaling. *Cell Metab.* **22**, 825–837 (2015).
20. I. Arias-Mayenco *et al.*, Acute O_2 sensing: Role of coenzyme QH_2/Q ratio and mitochondrial ROS compartmentalization. *Cell Metab.* **28**, 145–158.e4 (2018).
21. A. Moreno-Domínguez *et al.*, Acute O_2 sensing through HIF2α-dependent expression of atypical cytochrome oxidase subunits in arterial chemoreceptors. *Sci. Signal.* **13**, eaay9452 (2020).
22. C. H. Snyder, T. Merbitz-Zahradnik, T. A. Link, B. L. Trumpower, Role of the Rieske iron-sulfur protein midpoint potential in the protonmotive Q-cycle mechanism of the cytochrome bc1 complex. *J. Bioenerg. Biomembr.* **31**, 235–242 (1999).
23. F. Diaz, J. A. Enríquez, C. T. Moraes, Cells lacking Rieske iron-sulfur protein have a reactive oxygen species-associated decrease in respiratory complexes I and IV. *Mol. Cell. Biol.* **32**, 415–429 (2012).
24. L. A. Sena *et al.*, Mitochondria are required for antigen-specific T cell activation through reactive oxygen species signaling. *Immunity* **38**, 225–236 (2013).
25. G. B. Waypa *et al.*, Superoxide generated at mitochondrial complex III triggers acute responses to hypoxia in the pulmonary circulation. *Am. J. Respir. Crit. Care Med.* **187**, 424–432 (2013).
26. J. Lindeberg *et al.*, Transgenic expression of Cre recombinase from the tyrosine hydroxylase locus. *Genesis* **40**, 67–73 (2004).
27. M. I. Ekstrand *et al.*, Progressive parkinsonism in mice with respiratory-chain-deficient dopamine neurons. *Proc. Natl. Acad. Sci. U.S.A.* **104**, 1325–1330 (2007).
28. B. Díaz-Castro, C. O. Pintado, P. García-Flores, J. López-Barneo, J. I. Piruat, Differential impairment of catecholaminergic cell maturation and survival by genetic mitochondrial complex II dysfunction. *Mol. Cell. Biol.* **32**, 3347–3357 (2012).
29. F. Al Khazal *et al.*, Unexpected obesity, rather than tumorigenesis, in a conditional mouse model of mitochondrial complex II deficiency. *FASEB J.* **35**, e21227 (2021).
30. P. González-Rodríguez *et al.*, Disruption of mitochondrial complex I induces progressive parkinsonism. *Nature* **599**, 650–656 (2021).
31. J. Ureña, R. Fernández-Chacón, A. R. Benot, G. A. Alvarez de Toledo, J. López-Barneo, Hypoxia induces voltage-dependent Ca2+ entry and quantal dopamine secretion in carotid body glomus cells. *Proc. Natl. Acad. Sci. U.S.A.* **91**, 10208–10211 (1994).
32. B. Kadenbach, S. Arnold, A second mechanism of respiratory control. *FEBS Lett.* **447**, 131–134 (1999).
33. L. B. Sullivan *et al.*, Supporting aspartate biosynthesis is an essential function of respiration in proliferating cells. *Cell* **162**, 552–563 (2015).
34. H. Torres-Torrelo, P. Ortega-Sáenz, L. Gao, J. López-Barneo, Lactate sensing mechanisms in arterial chemoreceptor cells. *Nat. Commun.* **12**, 4166 (2021).
35. G. B. Waypa *et al.*, Hypoxia triggers subcellular compartmental redox signaling in vascular smooth muscle cells. *Circ. Res.* **106**, 526–535 (2010).
36. A. A. Starkov *et al.*, Mitochondrial alpha-ketoglutarate dehydrogenase complex generates reactive oxygen species. *J. Neurosci.* **24**, 7779–7788 (2004).
37. M. D. Brand, Riding the tiger–Physiological and pathological effects of superoxide and hydrogen peroxide generated in the mitochondrial matrix. *Crit. Rev. Biochem. Mol. Biol.* **55**, 592–661 (2020).
38. H. J. Timmers, W. Wieling, J. M. Karemaker, J. W. Lenders, Denervation of carotid baro- and chemoreceptors in humans. *J. Physiol.* **553**, 3–11 (2003).
39. D. Macias *et al.*, HIF-2alpha is essential for carotid body development and function. *eLife* **7**, e34681 (2018).
40. M. J. Wasicko, J. E. Melton, J. A. Neubauer, N. Krawciw, N. H. Edelman, Cervical sympathetic and phrenic nerve responses to progressive brain hypoxia. *J. Appl. Physiol.* **68**, 53–58 (1990).
41. E. T. Chouchani *et al.*, Ischaemic accumulation of succinate controls reperfusion injury through mitochondrial ROS. *Nature* **515**, 431–435 (2014).
42. C. M. Bisbach *et al.*, Succinate can shuttle reducing power from the hypoxic retina to the O_2-rich pigment epithelium. *Cell Rep.* **31**, 107606 (2020).
43. J. B. Spinelli *et al.*, Fumarate is a terminal electron acceptor in the mammalian electron transport chain. *Science* **374**, 1227–1237 (2021).
44. M. Shirahata, S. Andronikou, S. Lahiri, Differential effects of oligomycin on carotid chemoreceptor responses to O2 and CO2 in the cat. *J. Appl. Physiol.* **63**, 2084–2092 (1987).
45. M. García-Fernández, P. Ortega-Sáenz, A. Castellano, J. López-Barneo, Mechanisms of low-glucose sensitivity in carotid body glomus cells. *Diabetes* **56**, 2893–2900 (2007).
46. N. Sommer *et al.*, Mitochondrial cytochrome redox states and respiration in acute pulmonary oxygen sensing. *Eur. Respir. J.* **36**, 1056–1066 (2010).
47. N. Sommer *et al.*, Mitochondrial complex IV subunit 4 isoform 2 is essential for acute pulmonary oxygen sensing. *Circ. Res.* **121**, 424–438 (2017).
48. G. B. Waypa, N. S. Chandel, P. T. Schumacker, Model for hypoxic pulmonary vasoconstriction involving mitochondrial oxygen sensing. *Circ. Res.* **88**, 1259–1266 (2001).
49. E. D. Michelakis, B. Thébaud, E. K. Weir, S. L. Archer, Hypoxic pulmonary vasoconstriction: Redox regulation of O_2-sensitive K+ channels by a mitochondrial O_2-sensor in resistance artery smooth muscle cells. *J. Mol. Cell. Cardiol.* **37**, 1119–1136 (2004).
50. K. J. Dunham-Snary *et al.*, Ndufs2, a core subunit of mitochondrial complex I, is essential for acute oxygen-sensing and hypoxic pulmonary vasoconstriction. *Circ. Res.* **124**, 1727–1746 (2019).
51. T. Zera, D. J. A. Moraes, M. P. da Silva, J. P. Fisher, J. F. R. Paton, The logic of carotid body connectivity to the brain. *Physiology (Bethesda)* **34**, 264–282 (2019).
52. P. Ortega-Sáenz, C. Caballero, L. Gao, J. López-Barneo, Testing acute oxygen sensing in genetically modified mice: Plethysmography and amperometry. *Methods Mol. Biol.* **1742**, 139–153 (2018).
53. P. Ortega-Sáenz *et al.*, Carotid body chemosensory responses in mice deficient of TASK channels. *J. Gen. Physiol.* **135**, 379–392 (2010).
54. A. M. Muñoz-Cabello, H. Torres-Torrelo, I. Arias-Mayenco, P. Ortega-Sáenz, J. López-Barneo, Monitoring functional responses to hypoxia in single carotid body cells. *Methods Mol. Biol.* **1742**, 125–137 (2018).
55. L. Gao, I. Arias-Mayenco, P. Ortega-Sáenz, J. López-Barneo, Using redox-sensitive fluorescent probes to record real-time reactive oxygen species production in cells from mouse carotid body slices. *STAR Protoc* **2**, 100535 (2021).